JOURNAL OF CATALYSIS **178,** 315–327 (1998)
ARTICLE NO. CA982103

Oxidative Dehydrogenation of Ethane over a Pt-Coated Monolith versus Pt-Loaded Pellets: Surface Area and Thermal Effects

Derrick W. Flick and Marylin C. Huff[1]

Department of Chemical Engineering, University of Delaware, Newark, Delaware 19716

Received January 12, 1998; accepted April 16, 1998

The catalytic performance of Pt-coated γ-Al_2O_3 pellets is compared to the performance of a Pt-coated α-Al_2O_3 monolith in the oxidative dehydrogenation of ethane to ethylene at short contact times. The use of the high surface area γ-Al_2O_3 support has a detrimental impact upon the production of the desired reactive intermediate, C_2H_4. The porous nature of the high surface area pellet support reduces the selectivity to intermediate products (C_2H_4) in favor of complete combustion. The axial and radial temperature profiles of the monolith and packed bed were examined to better understand the difference in catalytic performance of the two catalyst configurations. The radial temperature profile for the Pt-coated γ-Al_2O_3 pellets shows hot spot formation along the center-line of the catalyst bed which leads to lower C_2H_4 selectivity and can lead to thermal runaway. However, the radial temperature profile of the Pt-coated α-Al_2O_3 monolith is fairly flat across the monolith with a slight temperature drop between the edge of the catalyst and the reactor wall. This more uniform catalyst temperature leads to a higher production of C_2H_4.

1. INTRODUCTION

The oxidative dehydrogenation of ethane over Pt-coated monolith catalysts at short contact times has been investigated concerning the maximization of C_2H_4 production (1–9). This process has several advantages over the current routes to olefins. In contrast to the endothermic thermal pyrolysis process (steam cracking) (10–12), the highly exothermic partial oxidation process generates enough heat to significantly reduce or perhaps completely eliminate the need for additional process heat. The conventional steam cracking typically requires large furnaces, whereas the oxidation processes can operate autothermally in relatively small reactors with low operating and capital expense.

Several reasons for the success of the Pt-coated monolith for the oxidative dehydrogenation of ethane at short contact times have been suggested:

(1) Low surface area and low contact times lead to nearly ideal plug flow reactor (PFR) behavior characterized by a high Peclet (Pe) number. The Peclet number is defined as:

$$\mathrm{Pe} = \frac{u\,L}{D} \qquad [1]$$

where u is the linear velocity in the catalyst, L is the length of the catalyst bed, and D is the gas phase axial dispersion. High Peclet numbers favor the reactive intermediates in series reactions (13–15).

$$C_2H_6 \xrightarrow{O_2} C_2H_4 + H_2O \xrightarrow{O_2} CO_x + H_2O + H_2. \qquad [2]$$

(2) The high thermal conductivity of the monolith support leads to the conduction of reaction heat upstream, effectively preheating the reactants and leading to nearly isothermal operation near the adiabatic reaction temperature (9, 16–19). This high and uniform reaction temperature favors the reaction which has the higher activation energy in a parallel network (i.e., oxidative dehydrogenation) (13, 20):

$$C_2H_6 \begin{cases} \nearrow C_2H_4 + H_2O \\ \searrow CO + H_2 \end{cases} \qquad [3]$$

(3) The high thermal conductivity of the monolith also leads to small radial temperature gradients which reduce the risk of hot spots and lead to uniform catalytic activity across the entire catalyst cross section.

The open structure of the foam monolith leads to only a minor pressure drop across the catalyst. The surface area of the catalyst can be easily varied by the application of washcoats to increase the effective surface area of the low surface area base support. However, the foam monolith can be relatively fragile; fracturing of the monolith can occur by thermal expansion. For this reason, only monoliths made from a select number of oxides that have low thermal expansion coefficients are applicable to these studies where the catalyst temperature cycles between 25 and 1100°C in a matter of seconds. Currently, α-Al_2O_3 and ZrO_2 are the most robust oxides for this application that are commercially available (21, 22).

[1] To whom all correspondence should be addressed. E-mail: huff@che.udel.edu.

0021-9517/98 $25.00

In addition to Pt/α-Al_2O_3 monoliths, we also have investigated the use of a single layer of Pt eggshell coated γ-Al_2O_3 pellets as a catalyst for the oxidative dehydrogenation of ethane. This is a first step is making the transition between a foam monolith and a packed bed. Packed beds are more versatile than foam monoliths and, in some applications, the small particles that compose the packed bed may be easier to handle than a single, fragile monolithic unit. Removal for regeneration or replacement of a deactivated catalyst is easily accomplished with packed bed reactors. However, packed beds will support a greater temperature gradient than the relatively conductive monolith such that isothermal operation cannot be assumed in a packed bed where hot spots are a realistic concern. Typical packed beds also tend to have a substantial pressure drop across the bed. By using a single layer of 1/8 inch Pt coated pellets, we are examining the effect of support surface area and temperature profiles in the axial and radial direction while the pressure drop through the catalyst is nearly the same as the monolith.

2. EXPERIMENTAL

2.1. Reactor Configuration

The reactor is essentially identical to that previously described for the production of syngas (23) and oxidative dehydrogenation of light alkanes (1, 2). The reactor consists of a quartz tube with an inner diameter of 20 mm. The catalyst is sealed in the tube with high temperature silica–alumina felt which prevents the bypass of gases around the catalyst. To reduce the radiation heat loss in the axial and radial directions and to better approximate adiabatic operation, inert foam monoliths are placed in front and behind the catalyst as heat shields, and the reaction zone is externally insulated.

2.2. Catalyst Preparation

The monolith catalyst is prepared as described in previous experiments (1, 23) from a 45 pore per inch (ppi) ceramic foam monolith (92% α-Al_2O_3, 8% SiO_2) that is impregnated with a saturated solution of H_2PtCl_6, calcined in air, and reduced in H_2. This process results in loadings of approximately 5% Pt. Lower weight loadings are obtained by using a more dilute solution of H_2PtCl_6. All monoliths used measured 18 mm in diameter and are 3 mm deep. These monoliths are not washcoated and have a low surface area of 200 cm^2/g by BET surface area measurement using N_2 as the adsorbate (24).

The Pt coated pellets were obtained from Alfa-AESAR. The pellets were 1/8 inch (3 mm) in diameter and length and were loaded with 0.5 wt% Pt. The pellets are made of γ-Al_2O_3 and the platinum coating extends approximately 1 mm into the pellet. In our study, a single layer of Pt coated pellets was obtained by stacking 20 pellets together such that the flat faces of the pellet were perpendicular to the flow direction. This resulted in a catalyst bed that was approximately 18 mm in diameter and 3 mm deep. The BET surface area of the fresh catalyst measured by N_2 absorption was 82 m^2/g (24).

2.3. Reactor Operation

The gas flow for the reactor is controlled by Brooks electronic mass flow controllers with an accuracy of ± 0.06 SLPM for each component. The total feed flow rate is 2 SLPM which corresponds to an approximate contact time of 5 ms for the monolith catalyst and 4 ms for the single layer of pellet catalyst. For all the experiments, the reactor pressure is maintained at 1.2 atm (18 psi). The reaction occurs autothermally around 1000°C and a sample of the product gases is fed to a HP 6890 Gas Chromatograph (GC) through heated stainless steel lines. At steady state, with 20% N_2 dilution, the Peclet number for these experiments is calculated to be 7.5 ± 1.5 for both monolith and pellet catalysts.

While the reaction operates autothermally at steady state, an external heat source is necessary to ignite the reaction. After ignition, the external heat source is removed and steady state is established. After each change in feed conditions, the reactor is allowed to achieve steady state ($<$10 min) before analysis of the reaction products by the GC.

The feed gas consists of C_2H_6 and O_2 with N_2 as the diluent. The level of dilution ranged from 20 to 80%. The N_2 was used as an internal GC calibration standard. All product concentrations except H_2O are measured relative to GC calibration standards. The H_2O in the product is calculated by an oxygen atom balance. The remaining atom balances, carbon and hydrogen, closed to within $\pm 10\%$. In Fig. 1, the flammability range and operating region are shown for our reactor. Some experiments were conducted with the feed composition within the flammability limits. In these instances, it is important to realize that this is a flow system with linear velocities on the order of 0.6 m/s. These velocities exceed the flame speed and prevent homogeneous ignition (9, 25).

The reaction temperature was measured by a type K (chromel/alumel) thermocouple inserted from the rear of the reactor and placed at the center of the reactor tube between the catalyst and the rear radiation heat shield. The temperature at the front of the catalyst is measured by a type K thermocouple that is located between the catalyst and the front heat shield.

The temperature measured at the back of the catalyst, the reaction temperature, is a good measure of both the product gas phase temperature and the surface temperature of the rear face of the catalyst, since the gas phase and surface temperatures are approaching equilibrium at the catalyst exit.

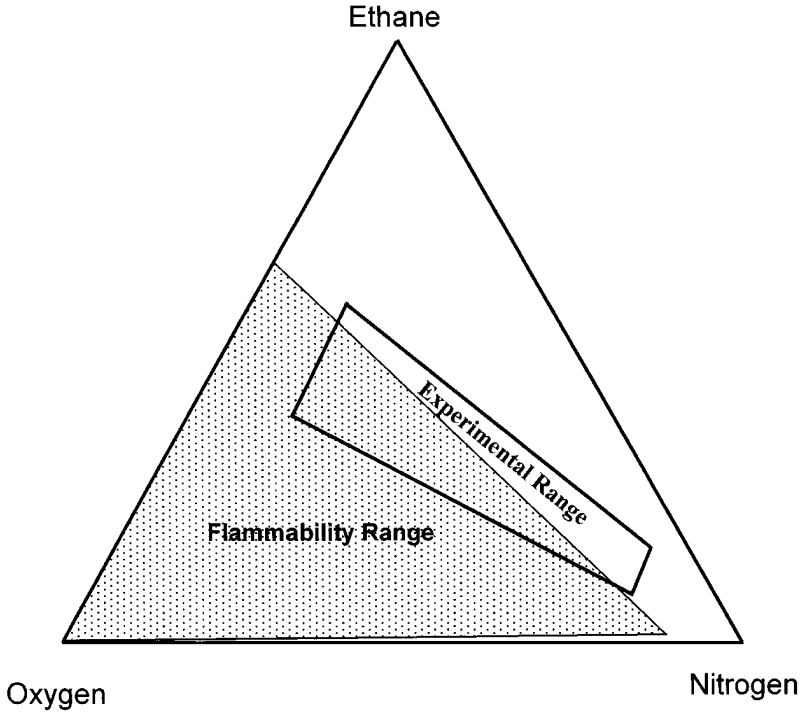

FIG. 1. Flammability limits for mixtures of ethane, oxygen, and nitrogen at atmospheric pressure and room temperature. The composition range within which all experiments were conducted is also shown.

However, the temperature measured at the front face of the catalyst is less reliable. Once the reaction is ignited, the front surface of the catalyst quickly reaches a temperature (∼1000°C) comparable to and often in excess of the temperature at the catalyst exit. This trend has been observed visually and quantified (in the absence of insulation) using optical pyrometry (26, 27). The thermocouple at the catalyst entrance, however, is seldom in intimate contact with the catalyst surface and instead measures the gas phase temperature of the reactant feed. The feed gas is preheated by radiation from the glowing catalyst and by contact with the front radiation shield that is also heated by radiation from the glowing catalyst (9, 16–18). Because of this, the catalyst entrance temperature is often a stronger function of the flow rate than of the actual catalyst surface temperature.

For each catalyst configuration, the temperature was measured in several additional places as shown in Fig. 2. For the single layer of pellets, the temperature was measured along the center-line of the catalyst bed at the front, rear, and midpoint of the pellet bed. The temperature was also measured at points that were one layer deep from the edge of the pellet bed, and between the pellets at the edge of the bed and the insulation on the inside of the reactor tube at the midpoint of the catalyst bed depth. For the single monolith catalyst, the temperature was measured at the center of the entrance and exit faces of the monolith, the side of the monolith embedded 1 mm into the side of the monolith at a position equidistant from the front and exit faces of the catalyst, and between the outside side edge of the monolith and the inside insulation. Due to the structure of the foam monolith, we are unable to measure the temperature at different positions along the center line of the monolith. However, if the single monolith is replaced by several thin monoliths, the temperature profile along the centerline of the reactor can be measured axially. For this study, three 3-mm monoliths, with approximately 0.7 wt% Pt, were stacked together to obtain the axial temperature profile for the reactor.

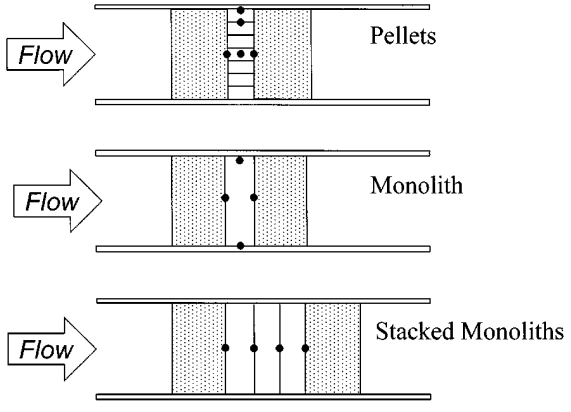

FIG. 2. Schematic diagrams of the different catalyst configurations; pellets (3 mm), single monolith (3 mm), and stacked monoliths (3 × 3 mm). The dots correspond to the placement of bare-wire chromel–alumel thermocouples in each of the different catalyst systems.

3. RESULTS

3.1. Transient Behavior of Pt/γ-Al_2O_3 Pellets

In Fig. 3 we show the results for ethane oxidation at a C_2H_6 : O_2 feed ratio of 1.8 and 20% N_2 over a single layer of 0.5 wt% Pt/γ-Al_2O_3 pellets as a function of time. This data was not collected continuously, but rather in segments of 6–10 h on consecutive days. At the end of a given day the reactor was shut down, going through a carbon-formation condition. The following day the reactor was restarted at the same conditions as the previous day. Any catalyst deactivation which occurred during the shut-down procedure on the previous day was regenerated within 10 min since the day-to-day agreement is excellent.

Figure 3a shows that the selectivities to C_2H_4 and CO drastically change during the first few hours of operation and slowly level off to steady state values after about 10 h of operation. The selectivities to CH_4 and CO_2 rise very slowly in the first several hours of operation and achieve steady state operation after approximately 10 h. Figure 3b shows that the H_2 selectivity also changes quickly in the first few hours and slowly levels off to steady values after 10 h. In contrast, the H_2O selectivity is fairly consistent over the entire time period with only a slight rise in the first 10 h. There is more scatter in the H_2O data since its composition is determined by mass balance than by direct measurement. Figure 3c shows that the C_2H_6 conversion rises very quickly to ~66% from 53% in the first 10 h of operation and then

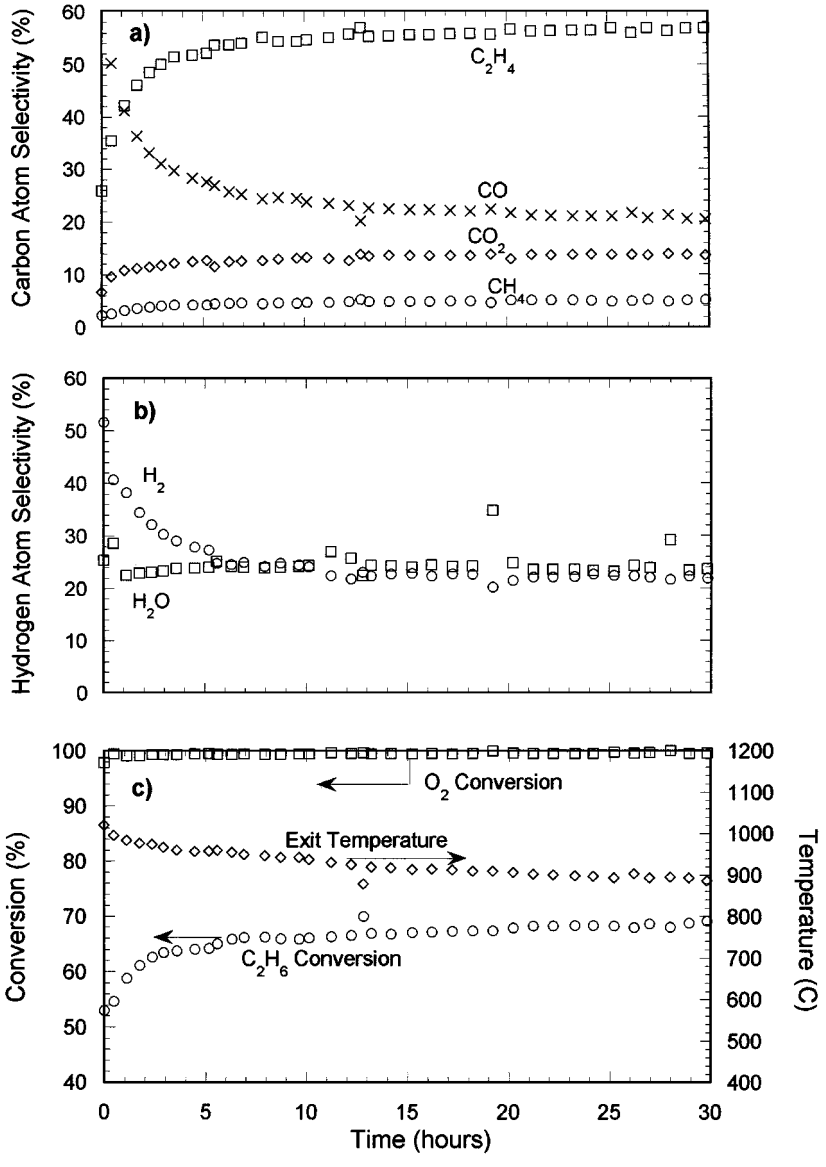

FIG. 3. Carbon atom and hydrogen atom selectivity (a, b), ethane and oxygen conversion (c), and catalyst temperature (c) for ethane oxidation over a single layer of 0.5 wt% Pt/γ-Al_2O_3 pellets as a function of the operation time at a C_2H_6 to O_2 ratio of 1.8 with 20% N_2 dilution with a total feed flow rate of 2 SLPM in an autothermal reactor at a pressure of 1.2 atm.

slowly climbs to ~70% after 20 h of operation. Except for the first data point where the oxygen conversion was 98%, the oxygen conversion was always greater than 99%. The catalyst exit temperature falls gradually from 1000°C to the steady state value of ~900°C after 10 h of operation. For all the selectivities and conversions, once the steady state values are reached, no change in selectivity or catalytic activity is observed for up to 50 h of operation.

3.2. Comparison of Pt/α-Al_2O_3 Monolith and Pt/γ-Al_2O_3 Pellets

3.2.1. Low Dilution

In Fig. 4 we show results as a function of the fuel-to-oxygen ratio for ethane oxidation over a 0.7 wt% Pt/α-Al_2O_3 foam monolith (solid lines) and a single layer of 0.5 wt% Pt/γ-Al_2O_3 pellets (dashed lines). Both catalyst beds were 3 mm thick. The monolith catalyst has a slightly higher weight loading of Pt. However, the amount of Pt on the monolith has little impact on the product slate. Due to the transient behavior exhibited over the pellets, the results are shown for the reactor once it has reached steady-state after approximately 30 h of operation. Figure 4a shows that the C_2H_4 selectivity over the monolith is slightly higher than over the pellets and increases at higher fuel-to-oxygen ratios. The CO selectivity over the two catalysts is essentially the same. The selectivity to CH_4 decreases with increasing fuel-to-oxygen ratio and is essentially the same for the 3 mm monolith and pellets. The selectivity to C_2H_2 also decreases with increasing fuel-to-oxygen ratio with significantly less

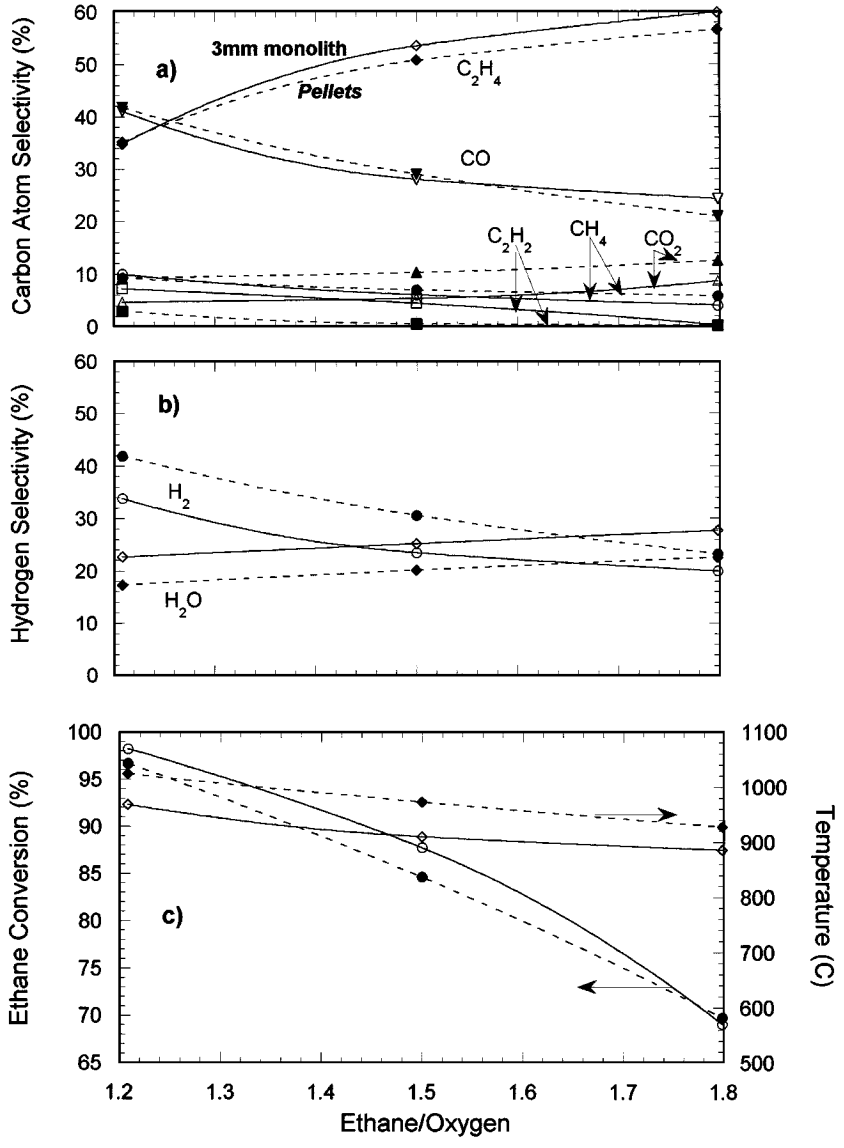

FIG. 4. Carbon atom and hydrogen atom selectivity (a, b), ethane conversion (c), and catalyst temperature (c) for ethane oxidation over a 45 ppi, 0.7 wt% Pt/α-Al_2O_3 monolith (solid line) and single layer of 0.5 wt% Pt/γ-Al_2O_3 pellets (dashed line) as a function of the C_2H_6 to O_2 ratio in the feed with 20% N_2 dilution with a total feed flow rate of 2 SLPM in an autothermal reactor at a pressure of 1.2 atm.

C_2H_2 produced over the pellets. In contrast, the selectivity to CO_2 increases with the fuel-to-oxygen ratio with significantly more CO_2 produced over the pellets. Figure 4b shows that the selectivities to H_2O and H_2 over the monolith and pellet catalyst parallel each other with more H_2 produced over the Pt/γ-Al_2O_3 pellets.

In Fig. 4c, the C_2H_6 conversion and rear, centerline temperature are shown for the two catalysts as a function of the fuel-to-oxygen ratio. The C_2H_6 conversion for both catalysts falls from >97% at a $C_2H_6 : O_2$ feed ratio of 1.2 to ~70% at a $C_2H_6 : O_2$ feed ratio of 1.8 with the conversion over the monolith slightly greater than the conversion over the pellets. The oxygen conversion also falls with increasing ethane composition, but it is always greater than 99%. Since the reactor operates nearly adiabatically, the temperature correspondingly falls with the decrease in conversion with increasing ethane concentration in the feed. The pellet catalyst has a slightly higher catalyst centerline exit temperature even at the lower ethane conversion.

Turnover frequencies can be calculated for both reactor configurations. Under these reaction conditions, at a $C_2H_6 : O_2$ feed ratio of 1.5, the turnover frequency for the pellets is ~0.7 s^{-1} and for the monolith is ~3000 s^{-1}. This assumes that the entire surface area of the fresh catalyst is being used for reaction. It is also important to note that experiments have been conducted using the monolith over a wide range of conditions (τ = 0.05 to 20 ms). All conditions lead to complete conversion of the oxygen. This casts serious doubt on the usefulness of a turnover frequency for the monolith.

3.2.2. *High Dilution*

High levels of reactant dilution have a dramatic effect on the reaction products for both reactor systems. In Fig. 5, we show the results for the two reactor configurations at a $C_2H_6 : O_2$ feed ratio of 1.8 with both 20 and 80% N_2 dilution. Changing the level of dilution from 20 to 80% decreases the catalyst exit temperature by more than 200°C. The oxygen conversion for the pellet catalyst is below 80% at high dilution while the oxygen conversion for the monolith reactor is always above 98% under the same conditions.

Under high dilution conditions, ethylene is not a major reaction product. Over the pellet catalyst, almost exclusively complete combustion products, CO_2 and H_2O, are

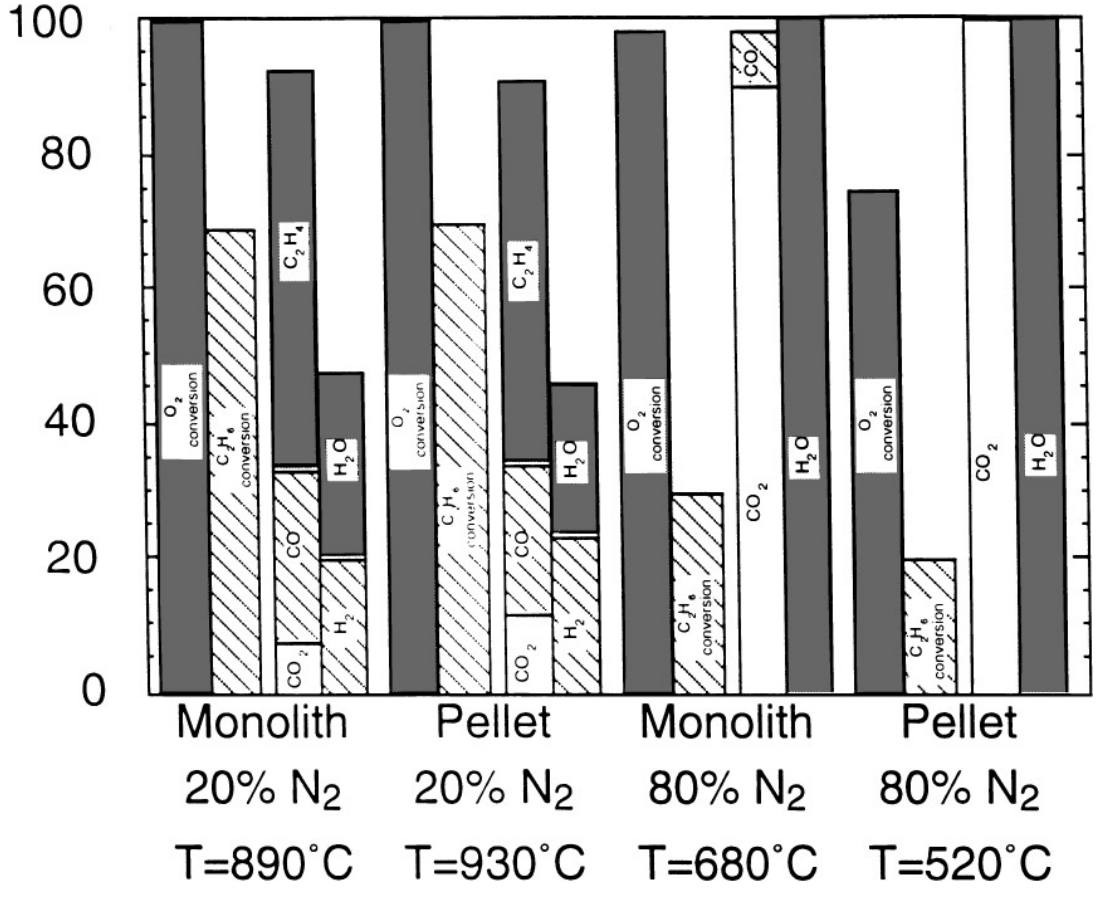

FIG. 5. Carbon atom and hydrogen atom selectivity and ethane and oxygen conversion for ethane oxidation over a 45 ppi, 0.7 wt% Pt/α-Al_2O_3 monolith and single layer of 0.5 wt% Pt/γ-Al_2O_3 pellets at both high (80% N_2) and low (20% N_2) dilution at a C_2H_6 to O_2 ratio in the feed of 1.8 with a total feed flow rate of 2 SLPM in an autothermal reactor at a pressure of 1.2 atm.

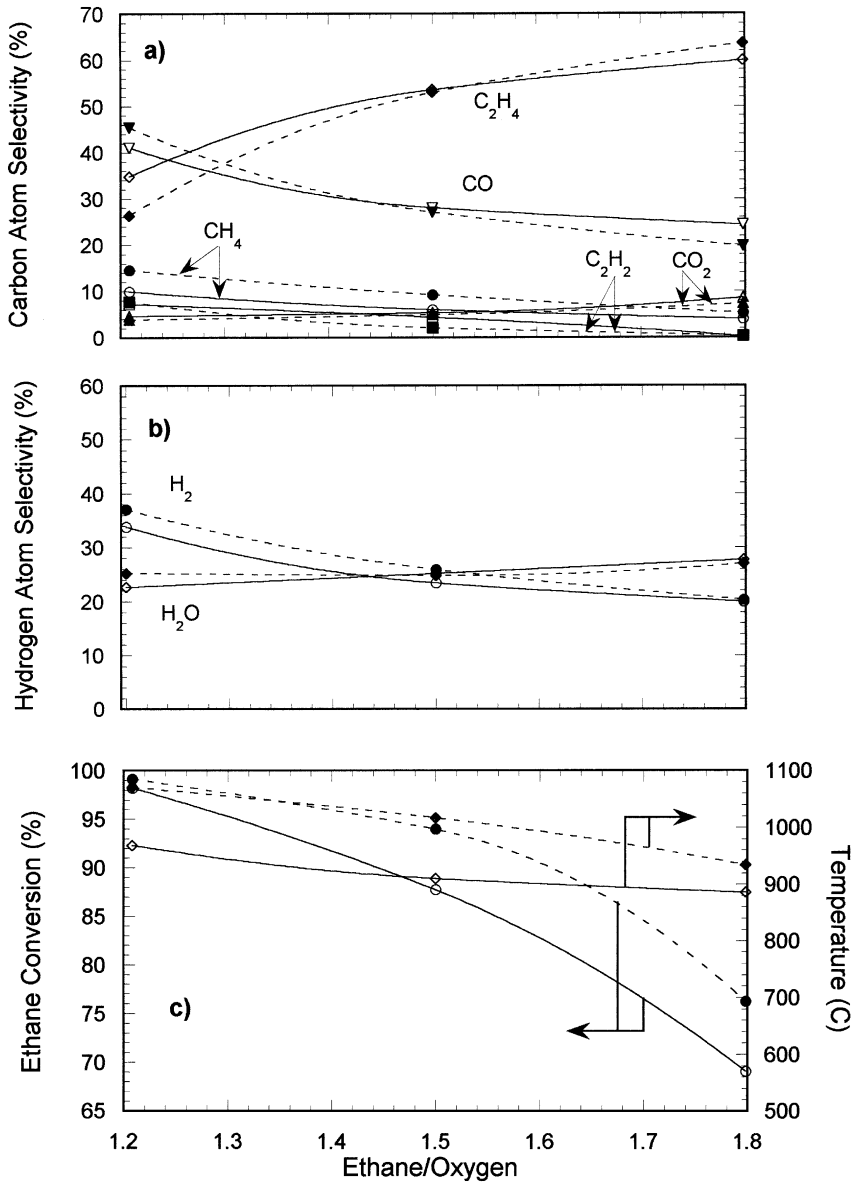

FIG. 6. Carbon atom and hydrogen atom selectivity (a, b), ethane and oxygen conversion (c), and catalyst temperature (c) for ethane oxidation over a 45 ppi, 0.7 wt% Pt/α-Al_2O_3 monolith (solid line) and a 45 ppi, 3.9 wt% Pt/α-Al_2O_3 monolith (dashed line) as a function of the C_2H_6 to O_2 ratio in the feed with 20% N_2 dilution with a total feed flow rate of 2 SLPM in an autothermal reactor at a pressure of 1.2 atm.

produced, while over the monolith, some CO and H_2 are also produced.

3.2.3. Pt Loading on the Monolith

The amount of Pt supported on the 3-mm α-Al_2O_3 monolith has little effect on the product selectivity. In Fig. 6, the carbon and hydrogen atom selectivity, ethane conversion, and rear centerline catalyst temperature are shown as a function of C_2H_6 : O_2 feed ratio with 20% N_2 dilution for foam monoliths with 3.93 wt% Pt (dashed) and 0.7 wt% Pt (solid). As shown in Fig. 6, the monolith with the higher weight loading has a slightly higher selectivity to CH_4 and H_2, along with a lower selectivity to C_2H_2. The selectivities for CO_2, H_2O, CO, and C_2H_4 are similar for the different catalyst loadings at the different feed conditions. The catalyst with the higher weight loading, however, shows a higher ethane conversion especially at the higher ethane compositions. The higher weight loading catalyst also shows a higher catalyst exit temperature. However, the product selectivities have a calculated error of $\pm 2.0\%$ and a calculated ethane conversion error of $\pm 4.0\%$. So with addition of the calculated errors, the amount of Pt loading on the α-Al_2O_3 monolith has only a minor effect upon the product selectivities and ethane conversion.

4. DISCUSSION

In summary, the pellet catalyst shows a long induction time before the reactor reaches steady state behavior. At both high and low nitrogen dilution, the pellet catalyst has a higher selectivity to CO_2 and corresponding lower selectivity for C_2H_4. At high nitrogen dilution, the pellet reactor also has a lower ethane and oxygen conversion than the monolith catalyst.

4.1. Induction Time in Pellet-Reactor

After reaction, the inside of the γ-Al_2O_3 pellets contain carbon deposits. These carbon deposits can be removed by oxidation. When the regenerated pellets are replaced in the reactor, they show a similar induction time trend. Therefore, we conclude that the carbon buildup in the interior of the pellets is largely responsible for the initial transient behavior of the catalyst. In Table 1, we show the amount of carbon deposited in the pellets for different operating times. The pellets rapidly gain carbon weight during the first several hours of operation which corresponds to the period with large product selectivity changes seen in the first few hours of operation as shown in Fig. 3. For one sample, the first six hours of operation accounted for 95% of the carbon weight gain.

Table 2 shows the operating conditions under which the carbon deposition takes place. At low nitrogen dilution, the carbon deposition is greater than at higher dilution. The amount of carbon deposited also increases with increasing ethane content in the feed at low nitrogen dilution. At 80% nitrogen dilution, only minor amounts of carbon were present after reaction. Thus, more carbon deposition takes place when there is a higher concentration of ethane in the feed which corresponds to conditions of low dilution and higher C_2H_6 : O_2 feed ratios.

4.2. Surface Area

Table 3 shows the BET surface area of the pellets measured by N_2 adsorption for the catalyst before reaction, after reaction, and after regeneration [24]. The surface area of the catalyst is greatly reduced during reaction, falling from 89 to 8 m^2/g after 50 h of operation. Therefore, the carbon buildup in the catalyst blocks a large portion of the interior pore space of the catalyst. This causes the highly porous γ-Al_2O_3 pellets to more closely resemble the low surface area α-Al_2O_3 monolith, which has a measured surface area of approximately 0.2 m^2/g. After regeneration, the surface area of the pellet is 72 m^2/g, indicating that during the high temperature reaction, the surface area of the γ-Al_2O_3 pellets decreases, but the support does not undergo a significant phase change to the low surface area phase, α-Al_2O_3, which is the thermodynamically stable phase at 1000°C. The decrease in the surface area is apparently due to the carbon blockage of the interior pores and not to the phase change to the γ-Al_2O_3 pellet.

The surface area of the catalyst can have an important influence on the product selectivities. The presence of a large pore structure in the catalyst can have a negative effect upon the production of reactive products. The reactive intermediates (C_2H_4) may be formed on the way into the catalyst pore. The reactive species can further react on the interior surface of the pore or encounter O_2 on its way out to form degradation products before the species has a chance to diffuse out of the pore and into the bulk gas phase. From the transient results for the pellets shown in Fig. 3, we observe that the partial oxidation product, CO, does fall drastically with operating time which corresponds to the formation of carbon deposits that lower the effective surface area of the catalyst pellets.

4.3. Oxygen Breakthrough and Reaction

The single layer of Pt/γ-Al_2O_3 pellets has large void channels between the stacked pellets where the gases can bypass

TABLE 1

Weight Gain per Pellet as a Function of Time for a Single Layer of 0.5 wt% Pt/γ-Al_2O_3 Pellets

Catalyst	Operation time (h)	Weight gain (mg/pellet)
γ-Al_2O_3 pellets	30	8.0
γ-Al_2O_3 pellets	6	7.0

Note. A single fresh pellet weighs 0.048 grams.

TABLE 2

The Weight Gain (mg) per Pellet at Different C_2H_6 to O_2 Ratios and N_2 Dilution in the Feed for Ethane Oxidation over a Single Layer of 0.5 wt% Pt/γ-Al_2O_3 Pellets

		Fuel : Oxygen ratio	
		1.2	1.8
Nitrogen dilution	20%	8.0	10.3
	80%	2.1	0.3

TABLE 3

The BET Surface Area of Pellet and Monolith Catalysts (24)

Catalyst	Surface area (m^2/g)
γ-Al_2O_3 pellet before reaction	89
γ-Al_2O_3 pellet after reaction	8
γ-Al_2O_3 pellet after regeneration	72
α-Al_2O_3 monolith after reaction	0.2

the catalyst. If there is oxygen breakthrough in the pellet catalyst, the oxygen will quickly react in combustion reactions in the hot product gases in the open reactor section behind the catalyst (1). The reactivity order of the major hydrocarbon components with oxygen in the product mixture is: $C_2H_2 > C_2H_4 > C_2H_6 > CH_4$ (28, 29). So if oxygen passes through the catalyst bed, it will quickly react with acetylene and ethylene via free radical homogeneous gas phase reactions, thereby reducing the selectivity to acetylene and ethylene and increasing the selectivity to CO_2.

If oxygen breakthrough occurs in the pellet catalyst, the product slate should show a higher selectivity to CO_2 and a corresponding lower selectivity to C_2H_2 and C_2H_4, which agrees with the results shown in Figs. 4 and 5. The selectivity to the most active species, C_2H_2, should show the largest reduction if there is oxygen available in the gas phase behind the catalyst. At a $C_2H_6:O_2$ feed ratio of 1.2 and 20% N_2 dilution, the C_2H_2 selectivity is less than half that seen for the monolith reactor at the same conditions. At a $C_2H_6:O_2$ feed ratio of 1.5 and 20% N_2 dilution, the C_2H_2 selectivity is reduced to only trace amounts in the product stream. As the availability of the most reactive species falls, the oxygen will begin to react with the next most reactive species, C_2H_4. At a $C_2H_6:O_2$ feed ratio of 1.5 and 20% N_2 dilution, the selectivity of C_2H_4 in the pellet reactor is lower than the monolith reactor. The same trend is also seen at a $C_2H_6:O_2$ feed ratio of 1.8 and 20% N_2 dilution.

At high nitrogen dilution (80% N_2 in the feed), the oxygen conversion for the pellet reactor is less than 80%, compared to almost complete oxygen conversion in the monolith reactor. Since oxygen is not completely consumed in the pellet reactor at high dilution, the most reactive species (C_2H_4, CO, and H_2) react with the remaining O_2 and the product contains almost exclusively complete combustion products.

4.4. Temperature

4.4.1. Radial Temperature Profile

In Fig. 7, the radial temperature profiles for the pellet reactor (dashed line) and the monolith reactor (solid line) are shown at low dilution (20% N_2 dilution) with a $C_2H_6:O_2$ feed ratio of 1.2. The radial temperature profile for the foam monolith catalyst is flat across the monolith with a slight temperature drop between the edge of the catalyst and the insulation. The temperature profile for the pellet bed shows a hot spot at the center of the bed with a steep temperature gradient to the reactor wall. The temperature at the center of the pellet bed is about 100°C higher than the temperature at the center of the monolith. The temperature between the catalyst and the insulation for the pellet bed, however, is lower than the monolith catalyst by approximately 70°C.

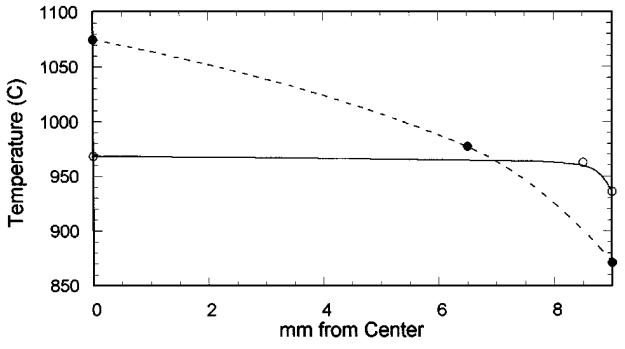

FIG. 7. The radial temperature profiles for the 3 mm, 45 ppi, 0.7 wt% Pt/α-Al_2O_3 monolith (solid line) and single layer of 0.5 wt% Pt/γ-Al_2O_3 pellets (dashed line) plotted as a function of the distance from the center-line of the reactor at a C_2H_6 to O_2 ratio of 1.2 in the feed with 20% N_2 dilution with a total feed flow rate of 2 SLPM in an autothermal reactor at a pressure of 1.2 atm.

4.4.2. Axial Temperature Profile

The axial temperature profiles for the pellet reactor under low and high dilution conditions are shown in Fig. 8. The temperature was measured at the front, exit, and midpoint of the catalyst bed center-line as shown in Fig. 2. At a $C_2H_6:O_2$ feed ratio of 1.2 and low dilution, the temperature increases slightly from the front of the catalyst to the center of the pellet bed and then falls to the catalyst exit. Whereas, at the higher $C_2H_6:O_2$ feed ratios and low dilution, the temperature is more nearly constant along the center-line of the catalyst. The temperature profile at high dilution is characterized by a temperature increase from the front of the catalyst to the center of the catalyst exit. Under high and low dilution conditions, the overall temperature of the catalyst decreases with increasing ethane content which agrees with the previous results for a monolith reactor (1, 2).

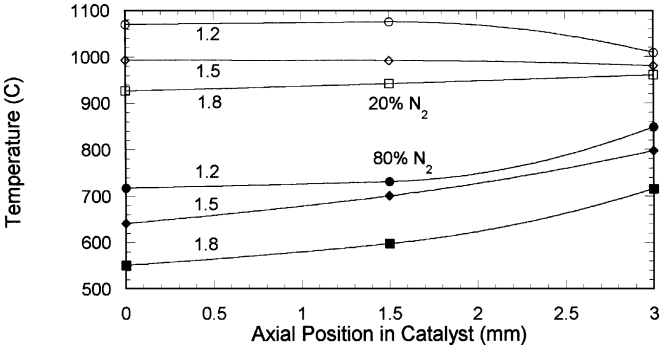

FIG. 8. The axial temperature profile along the center line of the reactor for a single layer of 0.5 wt% Pt/γ-Al_2O_3 pellets plotted as a function of the axial distance from the front of the catalyst at 2 SLPM and various C_2H_6 to O_2 ratios with 20% N_2 dilution and 80% N_2 dilution in an autothermal reactor at a pressure of 1.2 atm.

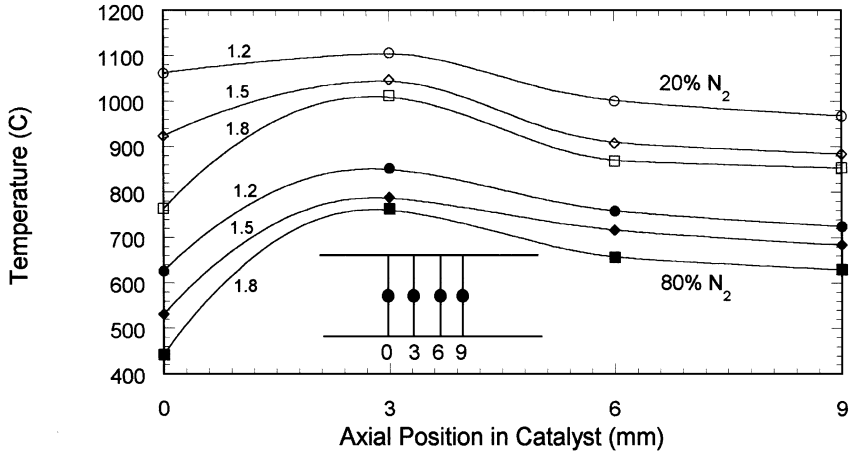

FIG. 9. Axial temperature profile along the center line of the reactor for a series of stacked monoliths plotted as a function of the axial distance from the front of the catalyst at 2 SLPM and various C_2H_6 to O_2 ratios with 20% N_2 dilution in an autothermal reactor at a pressure of 1.2 atm. Each α-Al_2O_3 monolith was 3 mm in length with 45 ppi and had a Pt loading of <1 wt%.

The axial temperature profiles for the series of stacked monoliths, which is three times the thickness of the pellet catalyst, under low dilution (20% N_2) conditions are shown in Fig. 9. For all compositions, the temperature profile for the stacked monolith reactor shows a characteristic shape. A similar axial temperature profile was observed for methane partial oxidation over a monolith supported catalyst in pilot plant experiments (30). At low nitrogen dilution, the temperature increases dramatically from the front of the first monolith to the front of the second monolith. The temperature then quickly falls 100–150°C before the front of the third monolith and then decreases slightly across the third monolith such that the exit temperature is 20–30°C lower than the temperature at the front of the third monolith.

It should be noted that the temperature measured at the front face of the first catalytic monolith is less reliable than the temperature measured elsewhere. The thermocouple at the catalyst entrance is seldom in intimate contact with the catalyst surface and, instead, measures the gas phase temperature of the reactant feed. The feed is preheated by radiation from the glowing catalyst and by contact with the front radiation shield that is also heated by radiation from the glowing catalyst (9, 16–18). Because of this, the catalyst entrance temperature is often a stronger function of the flow rate than of the actual catalyst surface temperature.

4.4.3. Temperature and Reaction

The oxidation reactions in this system are quite exothermic and lead to the high temperatures observed in this nearly adiabatic reactor. Previous studies of the monolith reactor for oxidative dehydrogenation proposed that the oxygen is quickly consumed by reaction in the front section of the catalyst (30, 31). This can be demonstrated by examining the axial temperature profile for the stacked monoliths (1). The temperature rises very quickly in the first monolith which corresponds to the consumption of oxygen by the exothermic oxidation. After the first monolith, the temperature in the catalyst falls, this can be due to heat loss through convection through the gas, conduction through the reactor walls, radiation from the glowing catalyst, and endothermic reactions, such as the thermal dehydrogenation of ethane.

The axial temperature profile for the Pt coated pellets at low dilution, 20% N_2, are relatively flat for $C_2H_6 : O_2$ feed ratios of 1.5 and 1.8. For a feed ratio of 1.2, the temperature falls as the gases proceed through the catalyst. The axial temperature profile for the pellets at high dilution, 80% N_2, however, shows an increase in temperature throughout the catalyst bed. If you apply the same logic stated above that the temperature continues to rise with the consumption of oxygen, the oxygen is still present in the gas and reacting on the catalyst at the exit of the bed. Therefore, there is the potential for oxygen in the product stream behind the catalyst. At the high temperatures present in the product gases behind the catalyst, the oxygen can undergo homogeneous reactions with reactive hydrocarbon species in the product mixture.

The radial temperature profile for the two catalysts provides evidence of possible hot spot formation in the pellet catalyst bed. The cross mixing of gases as they proceed through the tortuous foam monolith and the high thermal conductivity of the monolith, however, lead to a flatter radial temperature gradient which reduces the risk of hot spot formation. The sharp radial temperature profile in the pellet bed leads to a less selective product slate and the risk of catalyst deterioration at the centerline. The high temperature near the center of the reactor will favor C_2H_4 formation while the low temperature near the wall will favor CO_2 formation. This will lead to a gradient in O_2 concentration

which will further affect the local selectivity and temperature.

4.5. Energy Balance

The energy balance for the catalytic monolith can give additional insight into the temperature profiles, $T(z, r)$, for the reactor. The temperature profile within the reactor is a complex function of the thermal conductivity of the catalyst in the axial and radial directions, $k_{z\ \mathrm{eff,solid}}$ and $k_{r\ \mathrm{eff,solid}}$, the heat capacity of the gas phase, $C_{p,\mathrm{gas}}$, the heat of reaction, $\Delta H_{R,i}$, for each reaction, r_i, and heat transfer through the reactor walls, Q_{wall}. Assuming plug flow, the energy balance for the catalyst at steady state is

$$-k_{z\ \mathrm{eff,solid}}\left(\frac{\partial^2 T(z,r)}{\partial z^2}\right) - k_{r\ \mathrm{eff,solid}}\left(\frac{1}{r}\frac{\partial}{\partial r}\left(r\frac{\partial T(z,r)}{\partial r}\right)\right) + \rho v C_{p,\mathrm{gas}}\left(\frac{\partial T(z,r)}{\partial z}\right) = -\pi R^2 \sum_i (\Delta H_{R,i} \cdot r_i). \quad [4]$$

For a perfectly insulated reactor operating adiabatically, the system would have the following boundary conditions:

(1) The temperature along the centerline ($r = 0$) is finite and has a zero slope at the centerline:

$$\frac{\partial T}{\partial r} = 0 \quad \text{at } r = 0 \text{ for all } z. \quad [5]$$

(2) If the system is adiabatic, there is no heat loss through the reactor walls, $Q_{\mathrm{wall}} = 0$, and thus the heat flux at the walls is zero. This can be expressed by stating the slope of the temperature profile at the wall is zero:

$$\frac{\partial T}{\partial r} = 0 \quad \text{at } r = R \text{ for all } z. \quad [6]$$

(3) There is radiation heat loss in the axial direction from the catalyst at both the front ($z = 0$) and the exit ($z = L$). This can be expressed as

$$-k_{\mathrm{eff,solid}}\frac{\partial^2 T}{\partial z^2} + \rho v C_{p,\mathrm{gas}}\frac{\partial T}{\partial z} = -\pi R^2 \sum_i (\Delta H_{R,i} \cdot r_i) + Q_r \quad \text{at } z = 0 \text{ and } L, \quad [7]$$

where the heat transfer by radiation is $Q_r = \sigma T^4$ and σ is the Stefan–Boltzman constant (16).

4.5.1. Monolith

At steady state, we have measured nearly uniform temperatures in the radial direction and slight temperature gradients in the axial direction. Because of this observation, we simplify the heat transfer problem by assuming that the thermal conductivity of the solid is finite in the axial direction and infinite in the radial direction (32). So the simplified energy balance for the monolith catalyst operating adiabatically at steady state is

$$-k_{\mathrm{eff,solid}}\frac{d^2 T}{dz^2} + \rho v C_{p,\mathrm{gas}}\frac{dT}{dz} = -\pi R^2 \sum_i (\Delta H_{R,i} \cdot r_i). \quad [8]$$

This simplified energy balance is useful in understanding the axial temperature profile. Previous studies of the monolith reactor for oxidative dehydrogenation proposed that the oxygen is quickly consumed by highly exothermic oxidation reactions in the front section of the catalyst (30, 31). This generated heat can be dissipated by convection in the gas or heat loss through the walls of the reactor or consumed by endothermic reactions. Assuming that the reactor operates nearly adiabatically, the major portion of the heat generated by the exothermic reactions is converted into heating of the gases flowing through the catalyst or consumed in endothermic reactions after the oxygen is consumed (i.e., thermal dehydrogenation of unconverted ethane to ethylene.)

The experimental axial temperature profile showed a maximum gas phase temperature near the front of the catalyst followed by a slight cooling of the gases through the rest of the catalyst. Several items about the temperature profile for the monolith catalyst can be explained by examining the simplified energy balance for the adiabatic reactor:

(1) The axial temperature profile is not flat, but at a relatively high temperature which agrees with the assumption that the monolith displays a finite heat transfer in the axial direction.

(2) Convection of heat by the gas phase plays a very important role in this reactor. This can be directly observed by looking at the very sharp temperature increase near the front of the catalyst where the majority of the exothermic reactions are taking place, followed by a gradual cooling of the gases through the rest of the catalyst. Thus, a large majority of the heat generated by reaction is carried away from the catalyst through gas phase convection.

(3) The assumption of infinite heat transfer in the monolith in the radial direction agrees with the flat experimental radial temperature profile.

4.5.2. Pellets

The energy balance for the Pt-coated γ-Al_2O_3 pellets is more complicated than the monolith catalyst. The simplifying assumption made for the monolith catalyst cannot be applied to the pellet catalyst. In the pellet catalyst bed the heat can only be conducted in the radial direction through points where the pellets are in direct contact with each

other and through radiative heat transfer. The flow pattern through the single layer of pellets also does not allow for good mixing of the gases to provide a uniform radial temperature profile. Therefore, the energy balance for the pellet catalyst can be expressed as

$$-k_{z\ \mathrm{eff,bed}}\left(\frac{\partial^2 T(z,r)}{\partial z^2}\right) - k_{r\ \mathrm{eff,bed}}\left(\frac{1}{r}\frac{\partial}{\partial r}\left(r\frac{\partial T(z,r)}{\partial r}\right)\right) + \rho v C_{p,\mathrm{gas}}\left(\frac{\partial T(z,r)}{\partial z}\right) = -\pi R^2 \sum_i (\Delta H_{R,i} \cdot r_i), \quad [9]$$

where the thermal conductivity is some effective thermal conductivity accounting for the resistance to heat transfer of the point contacts in the bed. The temperature will therefore vary both axially and radially. The energy balance gives some insight into the radial temperature profile. Since the heat generated by exothermic reactions on pellets near the center of the bed can only be transferred to the surrounding pellets through points of direct contact, the pellet catalyst and gas temperatures near the center of the bed should be higher than the gas and pellet temperatures near the edge of the catalyst bed where heat can be removed through conduction through the reactor walls.

5. CONCLUSIONS

The γ-Al_2O_3 pellets coated with 0.5 wt% Pt show a long induction time due to the buildup of carbon on the inside of the pellets. The majority of the carbon deposition takes place in the first 2–3 h of operation, but it takes approximately 10–30 h of operation for the reactor to achieve and maintain steady state behavior. The carbon deposition drastically lowers the effective surface area of the catalyst, which is still an order of magnitude greater then the Pt-coated α-Al_2O_3 monolith.

The experiments show that at both high and low nitrogen dilution, the Pt-coated pellet catalyst has a higher selectivity to CO_2 and corresponding lower selectivity for C_2H_4. At high nitrogen dilution, the pellet catalyst also has a lower ethane and oxygen conversion than the Pt-coated monolith.

The pellet catalyst has several characteristics which lead to the preferential production of combustion products over the oxidative dehydrogenation products. First, the pellet catalyst is Pt/γ-Al_2O_3 and the monolith is Pt/α-Al_2O_3. These different supports have significantly different surface areas and potentially different reactivities. At the contact times and Pt loadings used here, it is unlikely that the oxide surface contributes catalytically.

Second, the radial temperature profile provides important insight into the thermal behavior of the catalyst. The radial heat transfer in the pellet catalysts is severely restricted such that heat can only be conducted through the points where the pellets are in direct contact with each other and through radiative heat transfer. Also, the flow pattern through the single layer of pellets does not allow for a good mixing of the gases to provide a uniform temperature profile. Thus, the heat transfer limitations can lead to hot spot formation along the centerline of the pellet bed and low reaction temperature near the wall. This lower temperature thermodynamically favors complete combustion and the resulting CO_2 formation over the less exothermic oxidative dehydrogenation reaction.

The potential also exists for oxygen breakthrough due to the large void channels in the single layer of pellets. At the high temperatures present in the product gases behind the catalyst section of the reactor, the oxygen can react through homogenous free radical reactions with highly reactive hydrocarbon species, C_2H_2 and C_2H_4, to form CO and CO_2. All of these factors relating to the pellet catalyst and single layer catalyst bed configuration can lead to the reduction in the selectivity to the desired intermediate product, C_2H_4, in favor of complete combustion products.

REFERENCES

1. Flick, D. W., and Huff, M. C., *Catal. Lett.* **47**, 91–97 (1997).
2. Huff, M., and Schmidt, L. D., *J. Phys. Chem.* **97**, 11815–11822 (1993).
3. Witt, P. M., and Schmidt, L. D., *J. Catal.* **163**, 465–475 (1996).
4. Font Freide, J. J., Howard, M. J., and Lomas, T. A., U.S. Patent 4,940,826, British Petroleum Company p.l.c., England, 1990.
5. Font Freide, J. J., Howard, M. J., and Lomas, T. A., U.S. Patent 5,105,052, British Petroleum Company p.l.c., England, 1992.
6. Golunski, S. E., and Hayes, J. W., U.S. Patent 5,593,935, Johnson Matthey Public Limited Company, England, 1997.
7. Astbury, C. J., Griffiths, D. C., Howard, M. J., and Reid, I. A. B., U.S. Patent 5,382,741, British Petroleum Company p.l.c., UK, 1995.
8. Heck, R. M., and Flanagan, P., U.S. Patent 4,844,837, Englehard Corporation, USA, 1989.
9. Astbury, C. J., Griffiths, D. C., and Reid, I. A. B., U.S. Patent 5,625,111, BP Chemicals Ltd., UK, 1997.
10. Chernyshkova, F. A., *Russian J. Appl. Chem.* **67**, 480–486 (1994).
11. Albright, L. F., Crynes, B. L., and Corcoran, W. H. (Eds.), "Pyrolysis: Theory and Industrial Practice," Academic Press, New York, 1983.
12. Renjun, Z., "Fundamentals of Pyrolysis in Petrochemistry and Technology," Citic, Beijing, 1993.
13. Kung, H. H., *Adv. Catal.* **40**, 1–38 (1994).
14. Fromont, G. F., and Bishoff, K. B., "Chemical Reactor Analysis and Design," 2nd ed., Wiley, New York, 1990.
15. Bischoff, K. B., and Levenspiel, O., *Chem. Eng. Sci.* **17**, 257–264 (1962).
16. Hayes, R. E., and Kolaczkowski, S. T., *Chem. Eng. Sci.* **49**, 3587–3599 (1994).
17. Lee, S.-T., and Aris, R., *Chem. Eng. Sci.* **32**, 827–837 (1977).
18. Hayes, R. E., Kolaczkowshi, S. T., Thomas, W. J., and Titiloye, J., *Ind. Eng. Chem. Res.* **35**, 406–414 (1996).
19. Leyshon, D. W., and Bader, R. A., U.S. Patent 4,876,409, Atlantic Richfield Company, USA, 1989.
20. Pilling, M. J., Robertson, S. H., and Seakins, P. W., *J. Chem. Soc. Faraday Trans.* **91**, 4179–4188 (1995).

21. Sweeting, T. B., Norris, D. A., and Strom, L. A., *in* "Materials Research Society Symposium—Fall Meeting, Pittsburgh, PA, 1994," pp. 309–314.
22. Strom, L. A., Sweeting, T. B., Norris, D. A, and Morris, J. R., *in* "Material Research Society Symposium—Fall Meeting, Pittsburgh, PA, 1994," pp. 321–326.
23. Hickman, D. A., and Schmidt, L. D., *J. Catal.* **136**, 300–308 (1992).
24. Abrams, L., personal communication.
25. Bolk, J. W., Siccama, N. B., and Westerterp, K. R., *Chem. Eng. Sci.* **51**, (1996).
26. Goetsch, D. A., and Schmidt, L. D., U.S. Patent 5,654,491, Regents of the University of Minnesota, USA, 1997.
27. Hickman, D. A., Haupfear, E. A., and Schmidt, L. D., *Catal Lett.* **17**, 223–237 (1993).
28. Rota, R., Bonini, F., Morbidelli, M., and Carra, S., *Ind. Eng. Chem. Res.* **35**, 2127–2136 (1996).
29. Shamsi, A., *Ind. Eng. Chem. Res.* **32**, 1877–1881 (1993).
30. Hochmuth, J. K., *Appl. Catal. B: Environmental* **1**, 89–100 (1992).
31. Huff, M. C., and Schmidt, L. D., *AICHE J.* **42**, 3484–3497 (1996).
32. Hegedus, L. L., *AICHE J.* **21**, 849–853 (1975).